First-principles calculation of magnetoelastic coefficients and magnetostriction in the spinel ferrites $CoFe_2O_4$ and $NiFe_2O_4$

Daniel Fritsch*
H. H. Wills Physics Laboratory, University of Bristol, Tyndall Avenue, Bristol BS8 1TL, United Kingdom

Claude Ederer†
Materials Theory, ETH Zürich, Wolfgang-Pauli-Strasse 27, 8093 Zürich, Switzerland

(Received 4 May 2012; published 6 July 2012)

We present calculations of magnetostriction constants for the spinel ferrites $CoFe_2O_4$ and $NiFe_2O_4$ using density functional theory within the GGA + U approach. Special emphasis is devoted to the influence of different possible cation distributions on the B-site sublattice of the inverse spinel structure on the calculated elastic and magnetoelastic constants. We show that the resulting symmetry lowering has only a negligible effect on the elastic constants of both systems as well as on the magnetoelastic response of $NiFe_2O_4$, whereas the magnetoelastic response of $CoFe_2O_4$ depends more strongly on the specific cation arrangement. In all cases our calculated magnetostriction constants are in good agreement with available experimental data. Our work thus paves the way for more detailed first-principles studies regarding the effect of stoichiometry and cation inversion on the magnetostrictive properties of spinel ferrites.

DOI: 10.1103/PhysRevB.86.014406 PACS number(s): 75.80.+q, 71.15.Mb, 75.47.Lx

I. INTRODUCTION

Magnetostriction describes the deformation of a ferro- or ferrimagnetic material during a magnetization process.[1–7] Thereby, one can distinguish between the *spontaneous volume magnetostriction*, which is independent of the magnetic field direction, and the so-called *linear magnetostriction* which characterizes the change of length along a certain direction that depends on the orientation of the applied magnetic field. The same magnetoelastic interaction that causes magnetostriction also leads to changes in the magnetic anisotropy as function of an externally applied strain.

Magnetostrictive materials are very important for applications as magnetic field sensors and magneto-mechanical actuators, where a large (and often also preferably linear) magnetic field response is essential.[8] On the other hand magnetostriction also causes noise and frictional losses in magnetic transformer cores, so that in this context a minimization of magnetostriction is desirable.

$CoFe_2O_4$ (CFO) is known to have one of the largest magnetostrictions among magnetic materials that do not contain any resource-critical rare-earth elements.[9] It has thus recently come into focus for use in magnetostrictive-piezoelectric composites,[10–12] where the goal is to achieve cross coupling between magnetic and dielectric degrees of freedom. Due to its insulating character and high magnetic ordering temperature, CFO together with $NiFe_2O_4$ (NFO) and other spinel ferrites is also a very attractive candidate for spintronics applications, in particular for spin-filtering tunnel barriers.[13,14] For many of these applications, thin films of CFO and NFO are epitaxially grown on substrates with different lattice constants. The resulting substrate-induced strain can then lead to distinctly different properties of the thin films compared to the corresponding bulk materials.

In view of this, a good quantitative understanding of magnetoelastic properties of spinel ferrites, that provides a solid basis for the interpretation of experimental results and allows for further optimization of magnetostrictive properties, is highly desirable. In particular, the ability to accurately predict effects of cation off-stoichiometry or surface and interface effects can provide valuable insights into the fundamental mechanisms determining the observed properties.

In previous work we have shown that first-principles calculations based on density functional theory (DFT) provide a suitable description of the magnetoelastic properties of spinel ferrites,[15,16] thus demonstrating the feasibility of more detailed studies into strain-induced effects in thin-film structures composed of CFO and NFO. Here we extend our previous study, in order to provide a more comprehensive picture of the magnetoelastic response of CFO and NFO, in particular including first-principles calculations of the complete set of cubic magnetoelastic and magnetostrictive coefficients. Most importantly, we investigate the influence of different possible cation distributions on the spinel B-site sublattice on the magnetoelastic response of these materials. The purpose of the present work is to provide a first-principles-based description of magnetoelastic coupling in spinel ferrites that can be used as a basis for further studies of the effect of cation substitution or off-stoichiometry on the magnetostrictive properties of this important class of materials.

This paper is organized as follows. In Sec. II A the spinel crystal structure is discussed, with special emphasis on cation inversion and different possible cation arrangements on the B-site sublattice. A general overview of magnetoelastic theory in cubic and tetragonal crystals is given in Sec. II B. Section II C describes how we determine all elastic and magnetoelastic coefficients from total energy electronic structure calculations, while Sec. II D provides some more technical details of our calculations. Our results for CFO and NFO are presented in Sec. III, and our main conclusions are summarized in Sec. IV.

II. THEORETICAL BACKGROUND AND COMPUTATIONAL METHOD

A. Inverse spinel structure and different cation distributions

Both CFO and NFO crystallize in the cubic spinel structure (see Fig. 1), which belongs to space group $Fd\bar{3}m$ (No. 227). The spinel structure contains two inequivalent cation sites, a tetrahedrally coordinated A site and an octahedrally coordinated B-site. In the *normal* spinel structure each of these sites is occupied by a particular cation species (e.g., divalent Mn^{2+} on the A site and trivalent Fe^{3+} on the B site in the case of $MnFe_2O_4$). However, in the *inverse* spinel structure, the more abundant cation species (here: Fe^{3+}) occupies all A sites and 50% of the B-sites, with the remaining 50% of B-sites occupied by the less abundant cation species (here: Co^{2+} or Ni^{2+}). In practice, intermediate cases can also occur, characterized by an inversion parameter λ, ranging from $\lambda = 0$ for the *normal* spinel structure to $\lambda = 1$ for complete inversion.

Both CFO and NFO are experimentally found to be inverse spinels, with $\lambda \approx 1$ for NFO but only incomplete inversion for CFO (with λ between 0.76 and 0.93, depending strongly on sample preparation conditions).[9,18] Both materials are generally found to be perfectly cubic, with a random distribution of divalent and trivalent cations over the B-site sublattice. However, indications for short-range cation order on the B-sites have been reported recently for the case of NFO, both in bulk single crystals as well as in thin films.[19,20]

In the present work we represent the inverse spinel structure within a tetragonal unit cell containing 4 formula units (see also Ref. 21) using lattice vectors $\vec{a}_1 = (a/2, -a/2, 0)$, $\vec{a}_2 = (a/2, a/2, 0)$, and $\vec{a}_3 = (0, 0, c)$, so that $c/a = 1$ corresponds to the unstrained, nominally cubic case. By distributing equal amounts of Co (respectively Ni) and Fe on the 8 B-sites within this unit cell, 70 cation arrangements belonging to 8 different space groups can be generated. In the following we consider only the three high-symmetry arrangements shown in Figs. 2(a)–2(c), plus one additional low-energy configuration for CFO, corresponding to 75% inversion, shown in Fig. 2(d). The specific cation arrangements shown in Fig. 2 in combination with the periodic boundary conditions corresponding to the tetragonal lattice vectors reduce the space group symmetries to $P4_122$ (No. 91), $Imma$ (No. 74), and $P\bar{4}m2$ (No. 115) for the fully inverse configurations, and to $P1$ (No. 1) for the case with 75% inversion. As we have previously shown,[21] both $P4_122$ and $Imma$ correspond to low-energy configurations for the fully inverse case, with $P4_122$ slightly lower in energy than $Imma$ for both CFO and NFO, whereas the $P\bar{4}m2$ configuration is energetically much less favorable. The $P1$ structure represents a low-energy configuration for the case $\lambda = 0.75$.[21] We also note that the $P4_122$ configuration corresponds to the local structure suggested for the experimentally observed short-range order in NFO,[19,20] whereas the $Imma$ configuration is equivalent to the one used in our previous study of magnetoelastic effects in CFO and NFO.[15,16] The corresponding results for the elastic and magnetoelastic properties are included here for better comparison. In addition, we have reproduced the $Imma$ results using the larger tetragonal unit cell and a setup identical to that for all other configurations and did not find any quantitative differences compared to Ref. 15.

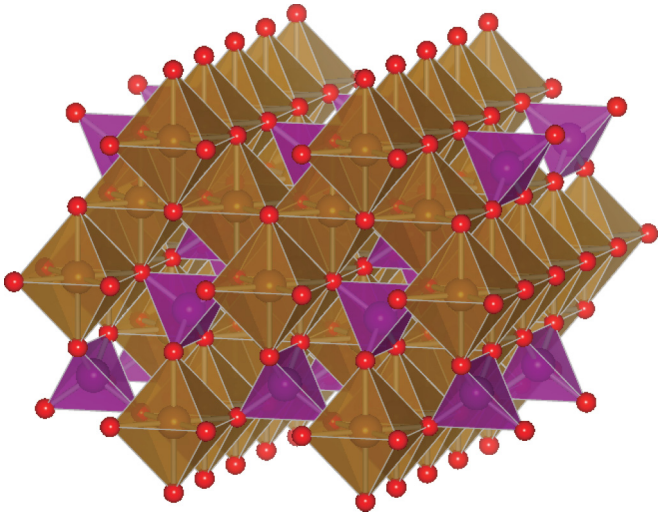

FIG. 1. (Color online) The spinel structure consists of an fcc network of oxygen anions (small red spheres) with cations occupying different interstitial sites of the fcc lattice, resulting in tetrahedrally coordinated A sites (purple) and octahedrally coordinated B-sites (brown). Picture has been reproduced from Fig. 1(a) in Ref. 15 and has been generated using VESTA (Ref. 17).

B. Magnetoelastic theory

Within the phenomenological theory of magnetoelasticity, the magnetoelastic energy density $f = E/V$ is expressed in terms of the direction cosines of the magnetization vector, α_i $(i = x, y, z)$, and the components of the strain tensor ε_{ij}, relative to a suitably chosen (nonmagnetic) reference state.[1–7] This energy density can be divided into a purely elastic term, f_{el}, and a magnetoelastic coupling term, f_{me}, which is usually taken as linear in the strain components. For a cubic crystal these terms have the following form:[22]

$$f_{\mathrm{el}}^{\mathrm{cubic}} = \tfrac{1}{2}C_{11}\left(\varepsilon_{xx}^2 + \varepsilon_{yy}^2 + \varepsilon_{zz}^2\right) + 2C_{44}\left(\varepsilon_{xy}^2 + \varepsilon_{yz}^2 + \varepsilon_{zx}^2\right) + C_{12}(\varepsilon_{yy}\varepsilon_{zz} + \varepsilon_{xx}\varepsilon_{zz} + \varepsilon_{xx}\varepsilon_{yy}) \quad (1)$$

and

$$f_{\mathrm{me}}^{\mathrm{cubic}} = B_0(\varepsilon_{xx} + \varepsilon_{yy} + \varepsilon_{zz}) + B_1\left(\alpha_x^2\varepsilon_{xx} + \alpha_y^2\varepsilon_{yy} + \alpha_z^2\varepsilon_{zz}\right) + 2B_2(\alpha_x\alpha_y\varepsilon_{xy} + \alpha_y\alpha_z\varepsilon_{yz} + \alpha_z\alpha_x\varepsilon_{zx}), \quad (2)$$

where C_{11}, C_{12}, and C_{44} are elastic and B_0, B_1, and B_2 are magnetoelastic coupling constants.

The relative length change along an arbitrary (measuring) direction with direction cosines β_i is given by

$$\frac{\Delta l}{l} = \sum_{i,j} \varepsilon_{ij}\beta_i\beta_j, \quad (3)$$

where the strain components depend on the magnetization directions. These equilibrium strains as a function of the magnetization direction can be found by minimizing the sum of the two energy expressions (1) and (2) with respect to all

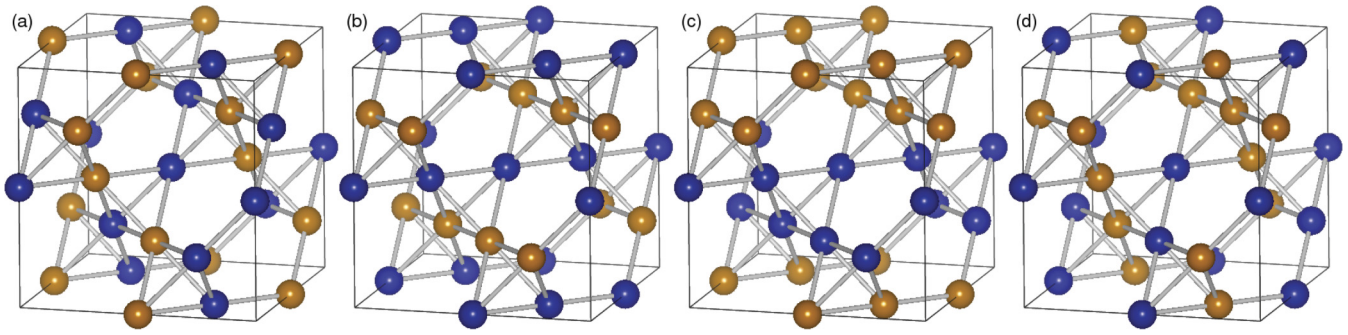

FIG. 2. (Color online) Cation distribution of Fe (brown/light gray) and Co (Ni) (blue/dark gray) on the B-sites of the spinel structure for the different configurations used in our calculations. Note that only the B sublattice is shown. From left to right the depicted structures correspond to space groups (a) $P4_122$ (No. 91), (b) $Imma$ (No. 74), and (c) $P\bar{4}m2$ (No. 115). Panel (d) on the right displays the CFO low-energy solution with incomplete degree of inversion, $\lambda = 0.75$, corresponding to space group $P1$ (No. 1) (Ref. 21). Pictures have been generated using VESTA (Ref. 17).

strain components. This results in

$$\left.\frac{\Delta l}{l}\right|_{\text{cubic}} = \lambda^{\alpha} + \frac{3}{2}\lambda_{100}\left(\alpha_x^2\beta_x^2 + \alpha_y^2\beta_y^2 + \alpha_z^2\beta_z^2 - {}^1\!/_3\right) + 3\lambda_{111}(\alpha_x\alpha_y\beta_x\beta_y + \alpha_y\alpha_z\beta_y\beta_z + \alpha_x\alpha_z\beta_x\beta_z). \tag{4}$$

Here, $\lambda^{\alpha} = -(B_0 + B_1/3)/(C_{11} + 2C_{12})$ describes a pure volume magnetostriction that is independent of the magnetization direction (this term is sometimes omitted from the above formula and is of no concern in the present work). The widely used magnetostriction constants of a cubic crystal are given by

$$\lambda_{100} = -\frac{2}{3}\frac{B_1}{C_{11} - C_{12}} \tag{5}$$

and

$$\lambda_{111} = -\frac{B_2}{3C_{44}}. \tag{6}$$

These two coefficients measure the fractional length change along the [100] ($\beta_x = 1, \beta_y = \beta_z = 0$) and [111] ($\beta_i = 1/\sqrt{3}$) directions, when the sample is magnetized to saturation along the [100] ($\alpha_x = 1, \alpha_y = \alpha_z = 0$) and [111] ($\alpha_i = 1/\sqrt{3}$) directions, relative to an ideal demagnetized reference state which is defined by $\langle\alpha_i^2\rangle = 1/3$ and $\langle\alpha_i\alpha_j\rangle = 0$. In a polycrystalline sample one can only measure a direction average over both λ_{100} and λ_{111} given by[2]

$$\lambda_S = \tfrac{2}{5}\lambda_{100} + \tfrac{3}{5}\lambda_{111}. \tag{7}$$

As noticed in Sec. II A, the cation arrangements used to describe the inverse spinel structure within our calculations lower the cubic symmetry of the ideal spinel structure to tetragonal ($P4_122$ and $P\bar{4}m2$), orthorhombic ($Imma$), or even triclinic ($P1$). A full first-principles description of magnetoelastic effects within these lower symmetries would require the calculation of 6 (9, 21) different elastic and 7 (12, 36) magnetoelastic coupling constants for the mentioned tetragonal (orthorhombic, triclinic) space groups, respectively.[4] Due to the resulting large computational effort, and considering the fact that experimentally both CFO and NFO are found to be cubic, we do not attempt such a full determination of all elastic and magnetoelastic coefficients within the lower symmetries, and instead evaluate our results using the relations for the cubic case described above (i.e., similar to our previous work in Refs. 15 and 16). To estimate the degree to which the lower symmetry affects our calculated coefficients, we also compare some of our data to the correct formulas corresponding to the lower symmetry. For simplicity we hereby restrict ourselves to the tetragonal case. The required equations are presented in the following.

Within the lower tetragonal symmetry there are six independent elastic and seven different magnetoelastic coupling constants, in contrast to the three elastic and three magnetoelastic coefficients in the cubic case.[4] The resulting expressions for f_{el} and f_{me} then read[6]

$$f_{\text{el}}^{\text{tet}} = \tfrac{1}{2}c_{11}\left(\varepsilon_{xx}^2 + \varepsilon_{yy}^2\right) + \tfrac{1}{2}c_{33}\varepsilon_{zz}^2 + c_{12}\varepsilon_{xx}\varepsilon_{yy} + c_{13}(\varepsilon_{xx} + \varepsilon_{yy})\varepsilon_{zz} + 2c_{44}\left(\varepsilon_{yz}^2 + \varepsilon_{xz}^2\right) + 2c_{66}\varepsilon_{xy}^2, \tag{8}$$

with c_{ij} denoting the six different tetragonal elastic constants, and

$$f_{\text{me}}^{\text{tet}} = b_{11}(\varepsilon_{xx} + \varepsilon_{yy}) + b_{12}\varepsilon_{zz} + b_{21}\left(\alpha_z^2 - {}^1\!/_3\right)(\varepsilon_{xx} + \varepsilon_{yy}) + b_{22}\left(\alpha_z^2 - {}^1\!/_3\right)\varepsilon_{zz} + \tfrac{1}{2}b_3\left(\alpha_x^2 - \alpha_y^2\right)(\varepsilon_{xx} - \varepsilon_{yy}) + b_3'\alpha_x\alpha_y\varepsilon_{xy} + b_4(\alpha_x\alpha_z\varepsilon_{xz} + \alpha_y\alpha_z\varepsilon_{yz}), \tag{9}$$

with the various b's denoting the seven different tetragonal magnetoelastic coupling constants. The corresponding cubic expressions (1) and (2) can then be obtained from (8) and (9) with the additional symmetry constraints $c_{11} = c_{33} = C_{11}$, $c_{12} = c_{13} = C_{12}$, $c_{44} = c_{66} = C_{44}$, $b_{11} = b_{12} = B_0 + {}^1\!/_3B_1$, $b_{22} = -2b_{21} = b_3 = B_1$, and $b_3' = b_4 = B_2$.

C. Determination of elastic and magnetoelastic constants

In order to determine the (cubic) elastic constants for CFO and NFO, we first perform a full structural relaxation of both systems. Similar to our previous investigations,[15,16,21] we thereby constrain the lattice vectors to "cubic" symmetry ($c/a = 1$) and fix the internal coordinates of the A and B cations to ideal values corresponding to the cubic spinel structure; i.e., we only allow for an optimization of the total volume and the oxygen positions. We then determine the three independent cubic elastic constants C_{11}, C_{12}, and C_{44} and the two cubic magnetoelastic coupling constants B_1 and B_2 by distorting the equilibrium crystal structure in three different ways: (i) isotropic volume expansion, (ii) constraining two of the three

lattice dimensions and relaxing the third ("epitaxial strain"), and (iii) by applying a volume-conserving shear strain.

(i) *Isotropic volume expansion*. The dependence of the total energy E_{tot} on the unit cell volume V provides the bulk modulus B, which is defined as

$$B = V_0 \left(\frac{\partial^2 E_{\text{tot}}}{\partial V^2} \right) \Big|_{(V=V_0)}, \tag{10}$$

with V_0 being the equilibrium volume. According to Eq. (1) the bulk modulus B of a cubic crystal can be expressed in terms of the elastic moduli C_{11} and C_{12} as follows:

$$B = \tfrac{1}{3}(C_{11} + 2C_{12}). \tag{11}$$

(ii) *Epitaxial strain*. We follow the approach of Ref. 15 to obtain a second independent elastic constant by applying *epitaxial strain*; i.e., we constrain the "in-plane" lattice constant to values ranging from -4% to $+4\%$ relative to the theoretical equilibrium lattice constant a_0, and we relax the "out-of-plane" lattice constant and all internal structural parameters of the oxygen anions. The relation between the relaxed out-of-plane strain $\varepsilon_\perp$ and the fixed in-plane strain $\varepsilon_{||}$ then defines the so-called two-dimensional Poisson ratio ν_{2D}. It follows from Eq. (1) that for a cubic system ν_{2D} is given as

$$\nu_{2D} = -\frac{\varepsilon_\perp}{\varepsilon_{||}} = 2\frac{C_{12}}{C_{11}}. \tag{12}$$

The elastic moduli C_{11} and C_{12} can then be obtained from Eqs. (11) and (12) using the bulk modulus and two-dimensional Poisson ratio calculated from DFT.

For the cation arrangements with tetragonal, orthorhombic, or triclinic symmetry depicted in Fig. 2 the ratio $\varepsilon_\perp/\varepsilon_{||}$ can be different for different orientations of "out-of-plane" and "in-plane" directions relative to the crystal axes. To quantify the resulting difference we perform calculations for two symmetry-inequivalent orientations of the applied strain $\varepsilon_{||}$. In particular we apply the epitaxial constraint first within the xy plane ($\varepsilon_{||} = \varepsilon_{xx} = \varepsilon_{yy}$ and $\varepsilon_\perp = \varepsilon_{zz}$) and then also within the yz plane ($\varepsilon_{||} = \varepsilon_{yy} = \varepsilon_{zz}$ and $\varepsilon_\perp = \varepsilon_{xx}$). Using the tetragonal energy expressions of Eqs. (8) and (9) together with the definition of ν_{2D} in Eq. (12) one obtains $\nu_{2D}^{(xy)} = 2c_{13}/c_{33}$ and $\nu_{2D}^{(yz)} = (c_{12} + c_{13})/c_{11}$ for these two cases. The difference between these two values for ν_{2D} thus gives a measure for the difference between c_{11} and c_{33} as well as between c_{12} and c_{13}.

To obtain the magnetoelastic coupling coefficient B_1 we monitor the total energy differences for different orientations of the magnetization as a function of the applied in-plane constraint $\varepsilon_{||}$ and relaxed out-of-plane strain $\varepsilon_\perp = -\nu_{2D}\varepsilon_{||}$. Using the cubic expression (2) for f_{me} one can see that the strain dependence of the energy density for all in-plane orientations of the magnetization is given by $B_1\varepsilon_{||}$, whereas the strain dependence for out-of-plane orientation is given by $-B_1\nu_{2D}\varepsilon_{||}$. The strain dependence of the total energy difference between out-of-plane versus in-plane orientation of the magnetization is thus given by[23]

$$\Delta E/V = -(\nu_{2D} + 1)B_1\varepsilon_\parallel. \tag{13}$$

The coefficient B_1 can therefore be obtained from the calculated strain-dependent magnetic anisotropy energies (MAEs) and the previously determined two-dimensional Poisson ratio ν_{2D}. While B_1 is not directly accessible by experimental investigations, it is related to the magnetostriction constant λ_{100} via Eq. (5).

In the tetragonal case the monitored strain dependence of the total energy difference between out-of-plane versus in-plane directions of the magnetization will depend on the orientation of "out-of-plane" and "in-plane" directions with respect to the tetragonal crystal axes. For the epitaxial constraint applied within the xy plane (i.e., $\varepsilon_\parallel = \varepsilon_{xx} = \varepsilon_{yy}$, leading to a Poisson ratio $\nu_{2D}^{(xy)} = 2c_{13}/c_{33}$) and using the tetragonal energy density [Eqs. (8) and (9)], the following expression for the strain dependence of the total energy difference between in-plane and out-of-plane magnetization can be obtained:

$$(\Delta E)^{(xy)}/V = \left(2b_{21} - \nu_{2D}^{(xy)} b_{22}\right)\varepsilon_\parallel, \tag{14}$$

which is valid for all in-plane orientations of the magnetization. In contrast, for the epitaxial constraint applied within the yz plane [i.e., $\varepsilon_{||} = \varepsilon_{yy} = \varepsilon_{zz}$, leading to a Poisson ratio $\nu_{2D}^{(yz)} = (c_{12} + c_{13})/c_{11}$] the resulting $(\Delta E)^{(yz)}/V$ depends on the specific in-plane direction and is given by

$$(\Delta E)^{(yz)}/V = \begin{cases} \left(-\frac{1}{2}b_3\left(\nu_{2D}^{(yz)} + 1\right) - \left(b_{21} + b_{22} - \nu_{2D}^{(yz)} b_{21}\right)\right)\varepsilon_\parallel & \text{for} \quad (\Delta E)^{(yz)} = E_{100} - E_{001}, \\ \left(-b_3\left(\nu_{2D}^{(yz)} + 1\right)\right)\varepsilon_\parallel & \text{for} \quad (\Delta E)^{(yz)} = E_{100} - E_{010}, \\ \left(-\frac{3}{4}b_3\left(\nu_{2D}^{(yz)} + 1\right) - \frac{1}{2}\left(b_{21} + b_{22} - \nu_{2D}^{(yz)} b_{21}\right)\right)\varepsilon_\parallel & \text{for} \quad (\Delta E)^{(yz)} = E_{100} - E_{011/01\bar{1}}. \end{cases} \tag{15}$$

(iii) *Volume-conserving shear strain*. The third cubic elastic modulus C_{44} is calculated according to Mehl,[24] by applying a volume-conserving monoclinic shear strain in the xy plane [$\varepsilon_\parallel = \varepsilon_{xy}$, $\varepsilon_\perp = \varepsilon_{zz} = \varepsilon_\parallel^2/(1 - \varepsilon_\parallel^2)$, $\varepsilon_{xx} = \varepsilon_{yy} = \varepsilon_{yz} = \varepsilon_{zx} = 0$]. The resulting change in total energy can then be written as

$$E(\pm\varepsilon_\parallel) = 2VC_{44}\varepsilon_\parallel^2 + O[\varepsilon_\parallel^4], \tag{16}$$

which allows for a straightforward determination of C_{44}.

For the cation arrangements with tetragonal, orthorhombic, or triclinic symmetry depicted in Fig. 2 different shear planes (ε_{xy}, ε_{yz}, ε_{zx}) are connected to different elastic moduli c_{ii}. Using the tetragonal energy expressions of Eqs. (8) and (9) together with the volume-conserving monoclinic strain in the xy plane described above, one notices the connection of ε_{xy} and c_{66}. However, choosing a volume-conserving monoclinic

strain in the yz plane [$\varepsilon_\parallel = \varepsilon_{yz}$, $\varepsilon_\perp = \varepsilon_{xx} = \varepsilon_\parallel^2/(1-\varepsilon_\parallel^2)$, $\varepsilon_{yy} = \varepsilon_{zz} = \varepsilon_{xy} = \varepsilon_{zx} = 0$] yields directly c_{44}, allowing for a comparison with c_{66}.

Similar to the first magnetoelastic coupling constant B_1, the second coefficient B_2 is determined by monitoring the total energy differences between different orientations of the magnetization as a function of the applied strain $\varepsilon_\parallel$. Depending on whether the shear strain $\varepsilon_\parallel$ is applied within the xy or yz plane, we consider the following energy differences:

$$(\Delta E)^{(xy)} = E_{110} - E_{100/010} = E_{100/010} - E_{1\bar{1}0}, \quad (17)$$

$$(\Delta E)^{(yz)} = E_{011} - E_{010/001} = E_{010/001} - E_{01\bar{1}}. \quad (18)$$

In all cases, the strain-dependence of these total energy differences can be written as

$$\Delta E/V = B_2 \varepsilon_\parallel. \quad (19)$$

Thus, the strain dependence of these energy differences is governed by the magnetoelastic coupling constant B_2, which can be determined from the calculated $\Delta E/V(\epsilon_\parallel)$.

Similar to B_1, the magnetoelastic coupling constant B_2 is also not directly accessible by experiment, but it is related to the magnetostriction constant λ_{111} via Eq. (6). Once the magnetostriction constants λ_{100} and λ_{111} are obtained, the average magnetostriction constant λ_S, suitable for polycrystalline samples, can be calculated from Eq. (7).

D. Other computational details

All calculations presented in this work are performed using the projector-augmented wave (PAW) method,[25] implemented in the Vienna *ab initio* simulation package (VASP 4.6).[26–29] Standard PAW potentials supplied with VASP were used in the calculations, contributing nine valence electrons per Co ($4s^2 3d^7$), 16 valence electrons per Ni ($3p^6 4s^2 3d^8$), 14 valence electrons per Fe ($3p^6 4s^2 3d^6$), and 6 valence electrons per O ($2s^2 2p^4$).

The generalized gradient approximation according to Perdew, Burke, and Ernzerhof (PBE)[30] is used in combination with the Hubbard "$+U$" correction,[31] where $U = 3$ eV and $J = 0$ eV is applied to the d states on all transition metal cations. We have shown in Refs. 15, 16, and 21 that this gives a realistic description of the electronic structure of CFO and NFO and leads to results which are in good overall agreement with available experimental data. Since here we are focusing on the comparison between various cation arrangements with different symmetries, we have not attempted a further optimization of the parameters U and J. Furthermore, we have verified that a variation of U within a reasonable range results only in small changes of the electronic structures of both CFO and NFO.

All structural relaxations are performed within a scalar-relativistic approximation, whereas spin-orbit coupling is included for the calculation of the MAEs. A plane wave energy cutoff of 500 eV is used, and the Brillouin zone is sampled using a Γ-centered $5 \times 5 \times 3$ k-point grid both for the structural optimization and for all total energy calculations. We have verified that all quantities of interest, in particular the magnetic anisotropy energies, are well converged for this k-point grid and plane wave energy cutoff.

III. RESULTS AND DISCUSSION

A. Structural properties

The equilibrium lattice constants a_0, bulk moduli B, two-dimensional Poisson ratios ν_{2D}, and resulting elastic constants C_{11} and C_{12} as well as C_{44} obtained for the different cation arrangements for both CFO and NFO are given in Table I. One notices that the calculated lattice constants for the two low-energy configurations $Imma$ and $P4_122$ are very similar to each other, and that the ones for the higher energy $P\bar{4}m2$ configuration and for the case with 75% inversion for CFO are slightly larger than that (by less than 0.2%). This increase in lattice constant is mirrored by a corresponding decrease in the bulk modulus (by about 3%). Overall, the variation of both bulk modulus and equilibrium lattice constant between different cation distributions is much smaller than the slight under- and overestimation of these quantities with respect to the experimental value, which is within the usual limits of the PBE$+U$ approach (see also Ref. 15).

It can also be seen that the difference in the two-dimensional Poisson ratios obtained for two different orientations of $\varepsilon_\perp$ is rather small and of magnitude similar to the differences between the various cation arrangements. This indicates that the symmetry lowering due to the different cation arrangements has only a small effect on the elastic properties, which can still to a good approximation be described by cubic elastic constants C_{11} and C_{12}.

TABLE I. Optimized equilibrium lattice constant a_0, bulk modulus B, two-dimensional Poisson ratio ν_{2D}, and elastic moduli C_{11}, C_{12}, and C_{44} for CFO and NFO, obtained for different cation arrangements and strain orientations ($\varepsilon_\perp = \varepsilon_{zz} = z$ and $\varepsilon_\perp = \varepsilon_{xx} = x$) in comparison to experimental data. The experimental ν_{2D} has been evaluated from Eq. (12) using the experimental elastic constants. $P1$ in the case of CFO refers to the low-energy solution with incomplete degree of inversion, $\lambda = 0.75$ (Ref. 21).

CFO	a_0 (Å)	B (GPa)	$\varepsilon_\perp$	ν_{2D}	C_{11} (GPa)	C_{12} (GPa)	C_{44} (GPa)
$Imma$[32]	8.463	172.3	z	1.132	242.5	137.3	94.9
			x	1.147	240.8	138.1	83.2
$P4_122$	8.464	170.8	z	1.129	240.7	135.9	84.7
			x	1.147	238.7	136.9	
$P\bar{4}m2$	8.473	168.0	z	1.132	236.4	133.8	92.3
			x	1.128	236.8	133.6	
$P1$	8.477	167.8	z	1.155	233.6	134.9	87.7
			x	1.146	234.6	134.4	
Exp. (Ref. 33)	8.392	185.7		1.167	257.1	150.0	85.3
NFO	a_0 (Å)	B (GPa)	$\varepsilon_\perp$	ν_{2D}	C_{11} (GPa)	C_{12} (GPa)	C_{44} (GPa)
$Imma$[32]	8.426	177.1	z	1.106	252.2	139.5	93.2
			x	1.115	251.2	140.0	87.6
$P4_122$	8.428	175.4	z	1.116	248.7	138.8	87.4
			x	1.116	248.7	138.8	
$P\bar{4}m2$	8.435	173.3	z	1.116	245.7	137.1	91.0
			x	1.102	247.3	136.3	
Exp. (Ref. 33)	8.339	198.2		1.177	273.1	160.7	82.3

Applying the volume-conserving monoclinic strain as described in Sec. II B yields the remaining elastic modulus C_{44} which is in very good agreement with the experimental values for both CFO and NFO. To evaluate the influence of different orientations of $\varepsilon_\perp$ on C_{44} we applied $\varepsilon_\perp = \varepsilon_{xy}$ and $\varepsilon_\perp = \varepsilon_{yz}$ with the respective $\varepsilon_\parallel$ to the low-energy orthorhombic $Imma$ symmetry. The difference in the obtained C_{44} is slightly larger compared to the difference in the C_{11} and C_{12}, but still within the typical uncertainties of first-principles methods.

Overall it appears that the agreement between the calculated and experimental lattice constants and elastic moduli is quite good and within the typical uncertainties of state-of-the-art first-principles methods. We note that all calculated values correspond to 0 K, whereas the experimental values listed in Table I were measured at room temperature. However, and more importantly, the uncertainties resulting from the symmetry-lowering cation arrangements are significantly smaller than the typical deviations between calculated values and experimental data. Therefore, the elastic properties of the various cation arrangements of lower symmetry can be well described by cubic elastic constants.

B. Magnetoelastic properties

1. NFO

Next we focus on the magnetoelastic coupling in NFO. The calculated MAEs necessary to determine the magnetoelastic coupling constant B_1 are depicted in Fig. 3. As described in Sec. II C these MAEs are defined here as the energy differences for various orientations of the magnetization with respect to the magnetization direction perpendicular to the applied strain plane, i.e., [001] for $\varepsilon_\parallel = \varepsilon_{xx} = \varepsilon_{yy}$ and [100] for $\varepsilon_\parallel = \varepsilon_{yy} = \varepsilon_{zz}$. According to Eq. (13) the slope of the curves given in Fig. 3 is directly related to the magnetoelastic coupling constants B_1. At first sight, the slopes of all curves in all panels are very similar and negative, thus leading to a positive B_1 (the range of the y axes is the same in all panels to allow for a direct inspection of slope differences).

In the tetragonal symmetries ($P4_122$ and $P\bar{4}m2$) all curves fall on top of each other for $\varepsilon_\perp = \varepsilon_{zz}$ (left panels), whereas there is a small offset between the curves in all other cases, due to the lower symmetry. In the even lower $Imma$ symmetry this offset is also present for $\varepsilon_\perp = \varepsilon_{zz}$. Nevertheless, the variation with strain is very similar in all cases, and the values for B_1, obtained by averaging over all curves corresponding to the same symmetry and strain orientation, are given in Table II. These values range from 6.1 MPa to 6.9 MPa, depending on the specific cation arrangement and strain orientation. Due to these rather small variations, we can conclude that the magnetostrictive response in NFO can to a good approximation be described as cubic.

Together with the respective elastic constants from Table I the magnetostriction constants λ_{100} can be obtained via Eq. (5), and are also listed in Table II. It can be seen that there is only a weak influence of either cation arrangement or different strain planes on the NFO magnetostriction constant λ_{100}, which ranges from -35.9×10^{-6} to -41.3×10^{-6}. This agrees perfectly with experimental data ranging from -36.0×10^{-6} to -50.9×10^{-6}.

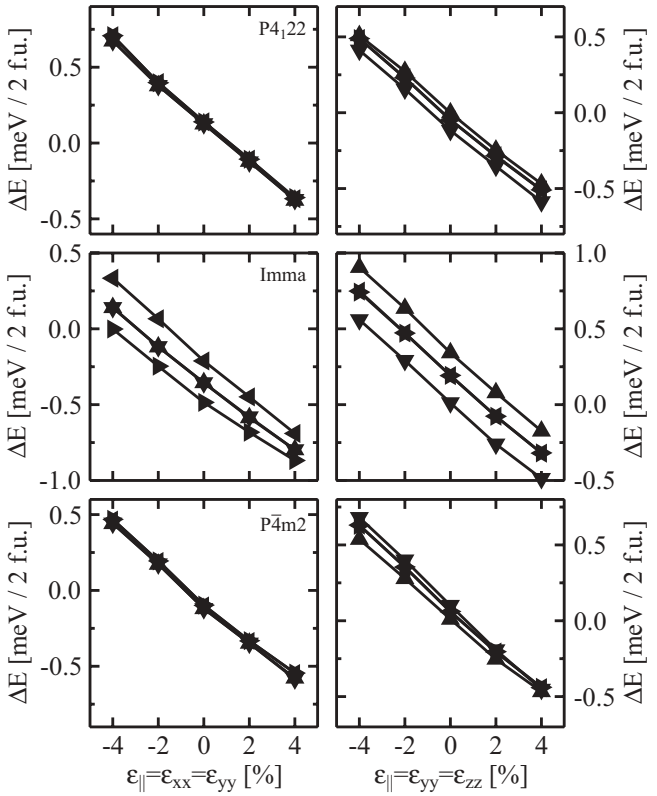

FIG. 3. Total energy difference ΔE per two formula units (f.u.) of NFO as a function of the epitaxial constraint $\varepsilon_\parallel$ for different cation arrangements. The left (right) panels correspond to the case with $\varepsilon_\perp = \varepsilon_{zz}$ ($\varepsilon_\perp = \varepsilon_{xx}$). The panels from top to bottom refer to symmetries $P4_122$, $Imma$ (see also Ref. 15), and $P\bar{4}m2$, respectively. In the case of $\varepsilon_\perp = \varepsilon_{zz}$ ($\varepsilon_\perp = \varepsilon_{xx}$) the depicted energy difference ΔE is taken with respect to the [001] ([100]) direction, with the symbols denoting ▲ [100] ([010]), ▼ [010] ([001]), ◀ [1$\bar{1}$0] ([01$\bar{1}$]), and ▶ [110] ([011]), respectively.

The calculated strain-dependent MAEs necessary for the determination of B_2 are shown in Fig. 4. The different curves

TABLE II. Magnetoelastic coupling constants (B_1, B_2) and magnetostriction constants (λ_{100}, λ_{111}, λ_S) for NFO using different cation arrangements and strain planes according to $\varepsilon_\perp = \varepsilon_{zz} = z$ ($\varepsilon_\perp = \varepsilon_{xx} = x$) in comparison with available experimental data. The average magnetostriction constant λ_S has been obtained using Eq. (7).

	$\varepsilon_\perp$	B_1 (MPa)	λ_{100} ($\times 10^{-6}$)	B_2 (MPa)	λ_{111} ($\times 10^{-6}$)	λ_S
$P4_122$	z	6.6	−40.1	2.5	−9.7	−21.9
	x	6.4	−38.6			
$Imma$[32]	z	6.1	−35.9	0.9	−3.4	−16.4
	x	6.7	−40.3	1.9	−7.3	−20.5
$P\bar{4}m2$	z	6.5	−40.0	1.4	−5.3	−19.2
	x	6.9	−41.3			
Exp.	Ref. 34[a]		−36.0		−4.0	−16.8
	Ref. 35[b]		−50.9		−23.8	−34.6
	Ref. 36[c]		−43.0		−20.1	−29.3

[a]Single crystals with $Ni_{0.8}Fe_{2.2}O_4$ composition (300 K).
[b]Single crystals of $NiFe_2O_4$ (4 K).
[c]Single crystals of $NiFe_2O_4$ (77 K).

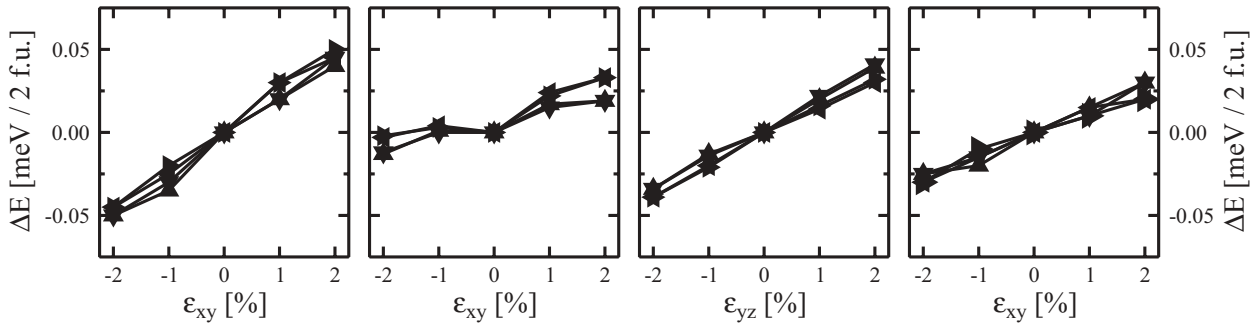

FIG. 4. Total energy difference ΔE per two formula units (f.u.) of NFO as function of shear strain for different cation arrangements. The panels from left to right refer to symmetries $P4_122$ ($\varepsilon_\parallel = \varepsilon_{xy}$), $Imma$ ($\varepsilon_\parallel = \varepsilon_{xy}$), $Imma$ ($\varepsilon_\parallel = \varepsilon_{yz}$), and $P\bar{4}m2$ ($\varepsilon_\parallel = \varepsilon_{xy}$), respectively. The depicted energy differences ΔE correspond to [110]-[100] (▲), [110]-[010] (▼), [100]-[1$\bar{1}$0] (►), and [010]-[1$\bar{1}$0] (◄), respectively, for $\varepsilon_\parallel = \varepsilon_{xy}$ and equivalent directions for $\varepsilon_\parallel = \varepsilon_{yz}$.

are adjusted to match at $\varepsilon_\parallel = 0$ in order to remove the corresponding offset which is irrelevant for the present work. The MAEs are chosen according to Eqs. (17) and (18) as energy differences between different in-plane orientations of the magnetization with respect to the applied shear strain $\varepsilon_\parallel$. According to Eq. (19) the slope of the curves given in Fig. 4 is directly related to the magnetoelastic coupling constant B_2. From Fig. 4 it can be seen that the slopes of these curves are positive, corresponding to positive B_2. There are slightly stronger nonlinearities in the curves in each of the panels compared to Fig. 3, as well as a stronger influence of the explicit cation arrangements. The resulting magnetoelastic coupling constants B_2 are listed in Table II and range from 0.9 MPa to 2.5 MPa, leading to magnetostriction constants λ_{111} ranging from -3.4×10^{-6} to -9.7×10^{-6}. These values are compatible with the lower experimental values, which themselves range from -4.0×10^{-6} to -23.8×10^{-6}. The last column in Table II also lists the averaged λ_S suitable for polycrystalline materials using Eq. (7).

Overall, the different cation arrangements and strain planes have only a rather weak influence on the calculated magnetostriction constants of NFO, which agree very well with the range of reported experimental data. We can therefore confirm our earlier finding,[15] that DFT + U methods are suitable for a quantitative description of magnetoelastic properties in this material. Moreover, although the symmetries of the investigated cation arrangements are not cubic, the magnetostrictive properties of NFO are very well described within the cubic theory.

2. CFO

Now we turn to our results for CFO. The calculated MAEs for the determination of the magnetoelastic coupling constant B_1 are depicted in Fig. 5. At first sight, one notices again that all slopes are negative, leading to a positive magnetoelastic coupling constant B_1. However, in contrast to NFO, the values are now much larger and also depend more strongly on the specific cation arrangement and orientation of the strain plane. In all cases except for the case of $P\bar{4}m2$ with $\varepsilon_\parallel = \varepsilon_{xx} = \varepsilon_{yy}$, we again obtain an offset between the different curves, which is due to the lower symmetry of the specific cation distribution. The differences in slopes observable between the various curves in the left panel of $P4_122$ symmetry are due to the fact

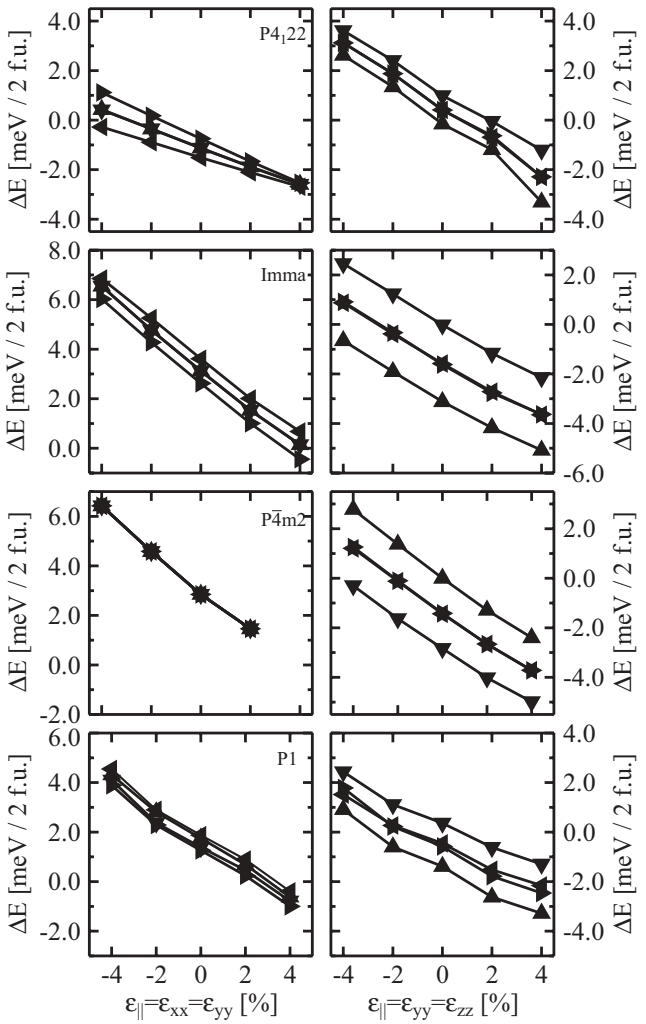

FIG. 5. Total energy difference ΔE per two formula units (f.u.) of CFO as function of the epitaxial constraint $\varepsilon_\parallel$ for different cation arrangements. The left (right) panels correspond to the case with $\varepsilon_\perp = \varepsilon_{zz}$ ($\varepsilon_\perp = \varepsilon_{xx}$). The panels from top to bottom refer to symmetries $P4_122$, $Imma$ (see also Ref. 15), and $P\bar{4}m2$, and $P1$ [low-energy solution for cation inversion $\lambda = 0.75$ (Ref. 21)]. In the case of $\varepsilon_\perp = \varepsilon_{zz}$ ($\varepsilon_\perp = \varepsilon_{xx}$) the depicted energy difference ΔE is taken with respect to the [001] ([100]) direction, with the symbols denoting ▲ [100] ([010]), ▼ [010] ([001]), ◄ [1$\bar{1}$0] ([01$\bar{1}$]), and ► [110] ([011]), respectively.

TABLE III. Magnetoelastic coupling constants (B_1, B_2) and magnetostriction constants (λ_{100}, λ_{111}, λ_S) for CFO using different cation arrangements and strain planes according to $\varepsilon_\perp = \varepsilon_{zz} = z$ ($\varepsilon_\perp = \varepsilon_{xx} = x$) in comparison with available experimental data. The average magnetostriction constant λ_S has been obtained using Eq. (7).

	$\varepsilon_\perp$	B_1 (MPa)	λ_{100} ($\times 10^{-6}$)	B_2 (MPa)	λ_{111} ($\times 10^{-6}$)	λ_S
$P4_122$	z	18.9	−120.1	−8.4	32.9	−28.3
	x	32.8	−215.0			
$Imma$[32]	z	39.7	−251.7	−11.6	40.9	−76.1
	x	29.2	−189.7	−12.2	48.8	
$P\bar{4}m2$	z	42.0	−272.7	−14.6	52.7	−77.5
	x	30.9	−199.4			
$P1$	z	29.1	−196.3	−7.6	28.8	−61.2
	x	24.2	−160.9			
Exp.	Ref. 37[a]		−225.0			
	Ref. 34[b]		−250.0			
	Ref. 34[c]		−590.0		120.0	−164.0

[a]Polycrystalline $CoFe_2O_4$ (300 K).
[b]Single crystals with $Co_{1.1}Fe_{1.9}O_4$ composition (300 K).
[c]Single crystals with $Co_{0.8}Fe_{2.2}O_4$ composition (300 K).

that in this case the system adopts an orbitally ordered ground state with symmetry lower than that of the underlying crystal structure. Strongest deviations from linearity are observed in the low-energy solution with symmetry $P1$ belonging to incomplete inversion $\lambda = 0.75$.

The determined magnetoelastic coupling constants B_1 are given in Table III, ranging from 18.9 MPa to 42.0 MPa. The largest influence of the strain plane orientation is observed for $P4_122$ symmetry. Overall, the specific cation arrangement has a much larger influence on the obtained magnetoelastic coupling constants in CFO compared to NFO. However, we note that even though there are pronounced differences between the two different strain orientations (left and right panels in Fig. 5) for the same cation arrangements, the strain dependence of the various calculated energy differences for the same strain orientation (different curves within each panel) are very similar in each case. From expression (15) for tetragonal symmetry, we can therefore empirically observe that the following approximate relationship holds between the various magnetoelastic coefficients:

$$\tfrac{1}{2}b_3(\nu_{2D}+1) \approx b_{21} + b_{22} - \nu_{2D}b_{21}. \tag{20}$$

However, since the slopes in the left and right panels of Fig. 5 differ, the stronger condition $b_3 = b_{22} = -2b_{21}$, which would be valid within cubic symmetry, is not fulfilled in CFO. The deviation from cubic symmetry caused by the specific cation arrangements is therefore more strongly manifested in the magnetoelastic response of CFO compared to NFO. Nevertheless, the approximate relation Eq. (20) indicates that some residue of the approximate structural cubic symmetry is still present also in the case of CFO.

The magnetostriction constants of CFO can now be obtained via Eq. (5) and using the elastic constants in Table I. The resulting values are listed in Table III and range from -120.1×10^{-6} to -272.7×10^{-6}. This agrees well with the lower range of available experimental data, which itself varies between -225×10^{-6} and -590×10^{-6}.

The strain-dependent MAEs necessary for the determination of B_2 are shown in Fig. 6, analogous to the NFO case. Most strikingly, and in contrast to NFO, the corresponding slope is negative, thus leading to a negative B_2 in CFO. The spread in slopes in each of the panels is comparable to NFO. While we obtain quite similar values for $Imma$ and $P\bar{4}m2$ symmetry (middle three panels), and also for $P4_122$ and $P1$, the latter two symmetries lead to somewhat smaller values for B_2 than the former.

Overall, B_2 ranges from −8.4 MPa to −14.6 MPa for the symmetries corresponding to complete cation inversion, and −7.6 MPa for the case with $\lambda = 0.75$ ($P1$). The resulting magnetostriction constants λ_{111} of CFO range from 28.8×10^{-6} to 52.7×10^{-6}, respectively. These values are lower than the (to the best of our knowledge only available) value of 120×10^{-6} reported experimentally.

In view of the relatively strong dependence on the specific cation arrangement, no particular trend is apparent on how the magnetostriction constants change with reduced cation inversion ($P1$ structure compared to the other cases with full inversion). Taking a closer look at the individual magnetostriction constants λ_{100} for all investigated cation arrangements and strain planes, one can notice that the largest magnetostriction occurs for cases where the cation species are arranged in alternating planes parallel to the applied strain

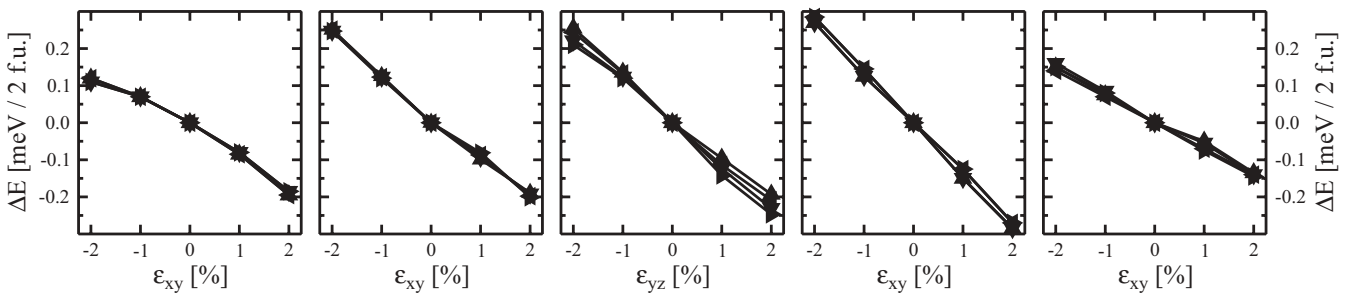

FIG. 6. Total energy difference ΔE per two formula units (f.u.) of CFO as function of shear strain for different cation arrangements. The panels from left to right refer to symmetries $P4_122$ ($\varepsilon_\parallel = \varepsilon_{xy}$), $Imma$ ($\varepsilon_\parallel = \varepsilon_{xy}$), $Imma$ ($\varepsilon_\parallel = \varepsilon_{yz}$), $P\bar{4}m2$ ($\varepsilon_\parallel = \varepsilon_{xy}$), and $P1$ [$\varepsilon_\parallel = \varepsilon_{xy}$, low-energy solution for cation inversion $\lambda = 0.75$ (Ref. 21)], respectively. The depicted energy differences ΔE correspond to [110]-[100] (▲), [110]-[010] (▼), [100]-[1$\bar{1}$0] (►), and [010]-[1$\bar{1}$0] (◄), respectively, for $\varepsilon_\parallel = \varepsilon_{xy}$ and equivalent directions for $\varepsilon_\parallel = \varepsilon_{yz}$.

plane, e.g., $\varepsilon_\perp = \varepsilon_{zz} = z$ for $Imma$ and $P\bar{4}m2$ symmetry (see Fig. 2). Furthermore, if one compares the two different strain orientations for $P4_122$ symmetry, the magnetostriction is larger for $\varepsilon_\perp = \varepsilon_{xx} = x$, where the strain plane contains chains of B-site cations with two equal cations next to each other in each chain. The magnetostriction value for the strain plane containing alternating cation chains within $P4_122$ symmetry is the smallest observed here. However, at present it is unclear whether these correlations between cation arrangement and λ_{100} are mostly coincidental, or whether they indeed indicate a deeper relationship between these two properties. In any case our results give clear evidence that a fully quantitative model of anisotropy and magnetostriction in CFO needs to include crystal- or ligand-field effects that go beyond the immediate nearest neighbor shell of the Co^{2+} cation.

The effect of different distributions of Co^{2+} and Fe^{3+} cations on the B-sites surrounding a specific Co B-site has been taken into account in the theory of magnetic anisotropy for CFO by Tachiki[38] and is also discussed by Slonczewski.[39] It was shown that the corresponding crystal-field component can have a strong effect on the resulting cubic magnetic anisotropy constants. The noticeable dependence of our calculated magnetoelastic coupling constants on the specific cation arrangement in CFO indicates that this crystal-field component is indeed quite strong and needs to be taken into account within a quantitative theory of anisotropy and magnetostriction in spinel ferrites.

IV. SUMMARY AND CONCLUSIONS

In summary, we have presented a detailed first-principles study of elastic and magnetoelastic properties of the inverse spinel ferrites NFO and CFO. We have calculated all cubic elastic and magnetoelastic constants from a variety of distorted crystal structures. Thereby, we have considered different possible cation arrangements to represent the inverse spinel structure, and in the case of CFO we also considered a cation distribution corresponding to incomplete inversion with $\lambda = 0.75$. The magnetoelastic coefficients are obtained from the strain dependence of the MAEs for two different deformations of the crystal structure.

Even though the symmetry of the considered cation arrangements is lower than cubic, our results show that the elastic response of both NFO and CFO can to a good approximation be described using cubic elastic constants. Since the elastic constants are mainly determined by the strength of the chemical bonding, this indicates that Co, Ni, and Fe all form bonds of similar strength with the surrounding atoms.

Similarly, the magnetoelastic response of NFO can also to a good approximation be described using the cubic expression for the magnetoelastic energy density [Eq. (2)]. This is indicated by the relatively small quantitative differences in the calculated magnetoelastic coefficients for the various cation arrangements. On the other hand, the magnetoelastic coefficients of CFO show a stronger dependence on the specific cation arrangement and the orientation of the applied strain, so that the cubic approximations is less justified in that case. In addition, the overall magnetoelastic response is much stronger in CFO than in NFO.

Both of these observations can be understood from the d^7 electron configuration of the Co^{2+} cation, which leads to stronger spin-orbit effects compared with the d^8 configuration of Ni^{2+}. In the latter, the orbital magnetic moment is strongly quenched by the dominant octahedral component of the crystal field, and the system is less sensitive to additional crystal-field components of lower symmetry. In contrast, the orbital moment is not fully quenched by the octahedral crystal field for the d^7 configuration of Co^{2+}, and additional splittings, which are created by the different arrangements of the surrounding B-site cations, can have much stronger effects on the electronic ground state within the partially filled minority-spin t_{2g} orbital manifold.

Both sign and magnitude of the calculated magnetostriction constants agree well with available experimental data. Even for CFO, where the calculated magnetostriction depends more strongly on the specific cation distribution than for NFO, the resulting uncertainty is within the spread of available experimental data.

Further experimental data for single crystals is therefore required for a more accurate comparison. We note that a number of obstacles can in principle affect an accurate comparison between theory and experiment. Apart from potential influences of varying sample stoichiometry, degree of inversion, and measuring temperature, the preparation of an ideal demagnetized state with an essentially random orientation of magnetic domains is relatively hard to achieve. For example, a state with 50% of domains oriented parallel and 50% of domains oriented antiparallel with respect to a certain axis would have zero magnetization but the magnetostrictive strain would already be saturated along that direction. Furthermore, for systems with very strong magnetic anisotropy, such as CFO, it can be very difficult to achieve full saturation along the hard direction.[40] Other sources of disagreement between theory and experiment could be due to the neglect of higher order terms in the energy expression (2),[2] or most likely due to deficiencies in the exchange correlation potential used in the DFT calculations. However, based on the currently available experimental data it can be concluded that the GGA + U method used in the present work is sufficiently accurate for further investigation on the effects of cation distribution, degree of inversion, and stoichiometry on the magnetostrictive properties of spinel ferrites.

Our work thus provides a sound basis for future investigations of magnetostriction and anisotropy in spinel ferrites as well as for future first-principles studies of magnetoelectric coupling in artificial multiferroic heterostructures containing either CFO or NFO in combination with ferroelectric and/or piezoelectric materials.

ACKNOWLEDGMENTS

This work was done mostly within the School of Physics at Trinity College Dublin, supported by Science Foundation Ireland under Ref. SFI-07/YI2/I1051 and made use of computational facilities provided by the Trinity Centre for High Performance Computing (TCHPC) and the Irish Centre for High-End Computing (ICHEC).

*daniel.fritsch@bristol.ac.uk; previous address: School of Physics, Trinity College, Dublin 2, Ireland.
†claude.ederer@mat.ethz.ch; previous address: School of Physics, Trinity College, Dublin 2, Ireland.

[1]C. Kittel, Rev. Mod. Phys. **21**, 541 (1949).
[2]E. W. Lee, Rep. Prog. Phys. **18**, 184 (1955).
[3]E. R. Callen and H. B. Callen, Phys. Rev. **129**, 578 (1963).
[4]E. Callen and H. B. Callen, Phys. Rev. **139**, A455 (1965).
[5]A. E. Clark, in *Ferromagnetic Materials*, edited by E. P. Wohlfarth (North-Holland, Amsterdam, 1980), Vol. 1, pp. 531–589.
[6]J. R. Cullen, A. E. Clark, and K. B. Hathaway, in *Materials, Science and Technology* (VCH Publishing, Weinheim, 1994), pp. 529–565.
[7]É. du Trémolet de Lacheisserie, in *Magnetism: Fundamentals*, edited by É. du Trémolet de Lacheisserie, D. Gignoux, and M. Schlenker (Springer, Boston, 2005), pp. 351–397.
[8]É. du Trémolet de Lacheisserie, in *Magnetism: Materials and Applications*, edited by É. du Trémolet de Lacheisserie, D. Gignoux, and M. Schlenker (Springer, Boston, 2005), pp. 213–234.
[9]V. A. M. Brabers, in *Handbook of Magnetic Materials*, edited by K. H. J. Buschow (Elsevier, New York, 1995), Vol. 8, pp. 189–324.
[10]H. Zheng, J. Wang, S. E. Loand, Z. Ma, L. Mohaddes-Ardabili, T. Zhao, L. Salamanca-Riba, S. R. Shinde, S. B. Ogale, F. Bai *et al.*, Science **303**, 661 (2004).
[11]F. Zavaliche, H. Zheng, L. Mohaddes-Ardabili, S. Y. Yang, Q. Zhan, P. Shafer, E. Reilly, R. Chopdekar, Y. Jia, P. Wright *et al.*, Nano Lett. **5**, 1793 (2005).
[12]N. Dix, R. Muralidharan, J.-M. Rebled, S. Estradé, F. Peiró, M. Varela, J. Fontcuberta, and F. Sánchez, ACS Nano **8**, 4955 (2010).
[13]M. G. Chapline and S. X. Wang, Phys. Rev. B **74**, 014418 (2006).
[14]U. Lüders, M. Bibes, K. Bouzehouane, E. Jacquet, J.-P. Contour, S. Fusil, J.-F. Bobo, J. Fontcuberta, A. Barthélémy, and A. Fert, Appl. Phys. Lett. **88**, 082505 (2006).
[15]D. Fritsch and C. Ederer, Phys. Rev. B **82**, 104117 (2010).
[16]D. Fritsch and C. Ederer, J. Phys.: Conf. Ser. **292**, 012014 (2011).
[17]K. Momma and F. Izumi, J. Appl. Cryst. **41**, 653 (2008).
[18]J. A. Moyer, C. A. F. Vaz, E. Negusse, D. A. Arena, and V. E. Henrich, Phys. Rev. B **83**, 035121 (2011).
[19]V. G. Ivanov, M. V. Abrashev, M. N. Iliev, M. M. Gospodinov, J. Meen, and M. I. Aroyo, Phys. Rev. B **82**, 024104 (2010).
[20]M. N. Iliev, D. Mazumdar, J. X. Ma, A. Gupta, F. Rigato, and J. Fontcuberta, Phys. Rev. B **83**, 014108 (2011).
[21]D. Fritsch and C. Ederer, Appl. Phys. Lett. **99**, 081916 (2011).
[22]We note that these expressions are in principle only valid for the cubic point groups $m3m$, $\bar{4}3m$, and 432.
[23]Note that we are not considering any strain-independent contributions to the magnetic anisotropy energy, which would lead to (strain-independent) differences between inequivalent in-plane directions.
[24]M. J. Mehl, Phys. Rev. B **47**, 2493 (1993).
[25]P. E. Blöchl, Phys. Rev. B **50**, 17953 (1994).
[26]G. Kresse and J. Hafner, Phys. Rev. B **47**, 558 (1993).
[27]G. Kresse and J. Hafner, Phys. Rev. B **49**, 14251 (1994).
[28]G. Kresse and J. Furthmüller, Comput. Mat. Sci. **6**, 15 (1996).
[29]G. Kresse and J. Furthmüller, Phys. Rev. B **54**, 11169 (1996).
[30]J. P. Perdew, K. Burke, and M. Ernzerhof, Phys. Rev. Lett. **77**, 3865 (1996).
[31]V. I. Anisimov, F. Aryasetiawan, and A. I. Liechtenstein, J. Phys.: Condens. Matter **9**, 767 (1997).
[32]We note that the lattice parameter a_0, the elastic constants B, ν_{2D}, C_{11}, and C_{12}, as well as the magnetoelastic constant B_1 and λ_{100} for *Imma* symmetry have already been published in Ref. 15. They are reproduced here for better comparison with the other cation distributions on the B-site sublattice.
[33]Z. Li, E. S. Fisher, J. Z. Liu, and M. V. Nevitt, J. Mater. Sci. **26**, 2621 (1991).
[34]R. M. Bozorth, E. F. Tilden, and A. J. Williams, Phys. Rev. **99**, 1788 (1955).
[35]A. B. Smith and R. V. Jones, J. Appl. Phys. **37**, 1001 (1966).
[36]K. I. Arai and N. Tsuya, J. Phys. Chem. Sol. **36**, 463 (1975).
[37]Y. Chen, J. E. Snyder, C. R. Schwichtenberg, K. W. Dennis, R. W. McCallum, and D. C. Jiles, IEEE Trans. Magn. **35**, 3652 (1999).
[38]M. Tachiki, Prog. Theor. Phys. **23**, 1055 (1960).
[39]J. C. Slonczewski, J. Appl. Phys. **32**, 253S (2010).
[40]M. Kriegisch, W. Ren, R. Sato-Turtelli, H. Müller, and R. Grössinger, J. Appl. Phys. **111**, 07E308 (2012).